Supporting Information

Centimeter-Level Double Perovskite Single Crystals with Strong Interlaminar Hydrogen Bonds for High-performance X-ray Detection

Linjie Wei,[a] *Yi Liu,**[a,b] *Yu Ma,*[a,b] *Qingshun Fan,*[a,b] *Liwei Tang,*[a,b] *Jingtian Zhang,*[a] *Junhua Luo*[a,b] *and Zhihua Sun**[a,b]

Experimental Section

Material preparation: The chemical reagents and solvents were purchased and used directly without further purification, including 4-aminomethyl-1-cyclohexane carboxylate (97%, Adamas), silver oxide (Ag_2O, 98%, Adamas), bismuth oxide (Bi_2O_3, 99.9%, Adamas), and hydroiodic acid (HI, 40%, Aladdin). Compound **1** was synthesized by mixing 4-aminomethyl-1-cyclohexane carboxylate, Ag_2O and Bi_2O_3 in concentrated hydroiodic acid solution according to stoichiometric ratio. At the beginning of the crystal growth, the saturated HI solution of 1 was prepared at 328 K and then maintained at 338 K for twelve hours. Subsequently, the high-quality crystal seed was slowly dipped into the solution and the top-seeded growth method was used for crystal growth. Large-size red crystals were obtained by the temperature cooling method from the saturated solution with a cooling rate of 1 K/day, as shown in Figures 1a and S1.

Material characterization: X-ray diffraction analysis was performed using the Bruker D8 diffractometer with the irradiation source Mo-Kα (λ = 0.77 Å). The single-crystal structure of **1** was obtained by direct method and refined by *SHELXTL* program using F^2 -based full matrix method. Powder XRD analysis was performed on a Rigaku (Mini Flex 600) X-ray diffractometer equipped with Co-Kα radiation. In addition, the absorption spectrum in the range of 200 to 900 nm was recorded using the PE Lambda 950 UV-VIS spectrophotometer.

Computational details: First-principles density function theory (DFT) calculations were performed using the plane-wave pseudopotential method implemented in the Cambridge Sequential Total Energy Package (CASTEP). The exchange-correlation effects were treated by the Perdew-Burke-Ernzerhof function for solids (PBEsol) in the generalized gradient approximation (GGA). The interactions between the ionic cores and the electrons were described by the norm-conserving pseudopotential. The orbital electrons of Ag ($4d^{10}5s^1$), Bi ($6s^26p^3$), I ($5s^25p^5$), C ($2s^22p^2$), N ($2s^22p^3$), and H ($1s^1$) were regarded as valence electrons.

Device fabrication: The vertical-type detectors were fabricated both perpendicular and

parallel to the (-100) crystal faces of the same single crystal. The surface was cleaned under nitrogen flow prior to device fabrication. Silver electrodes were evaporated onto opposite sides of the ~ 1 mm thick single crystals with an electrode area of ~1.1 mm^2 in the direction perpendicular to (-100) crystal face. Parallel to the (-100) plane, the spacing and area of the electrode are about 1.7 mm and 1.2 mm^2, respectively.

X-ray detection: The *I-V* and *I-t* curves under X-ray irradiation were recorded by using a Keithley 6517B high-precision electrometer. The photoelectric and X-ray detection measurements were conducted in a short time to exclude the influence of dark current drift on the response signal. The X-ray source is a commercially available silver target X-ray tube with photon energy up to 50 keV and peak intensity of 20 keV (4 W, Mini-X2, Amptek). By adjusting the tube current, the dose rate of the X-ray tube can be controlled and measured in integral mode using a commercial X-ray dosimeter (Accu-Gold, Radcal) attached to the ion chamber (10X 6-180 models).

[CCDC 2388392 contains the supplementary crystallographic data for this paper. These data can be obtained free of charge from The Cambridge Crystallographic Data Centre via www.ccdc.cam.ac.uk/data_request/cif.]

Figure

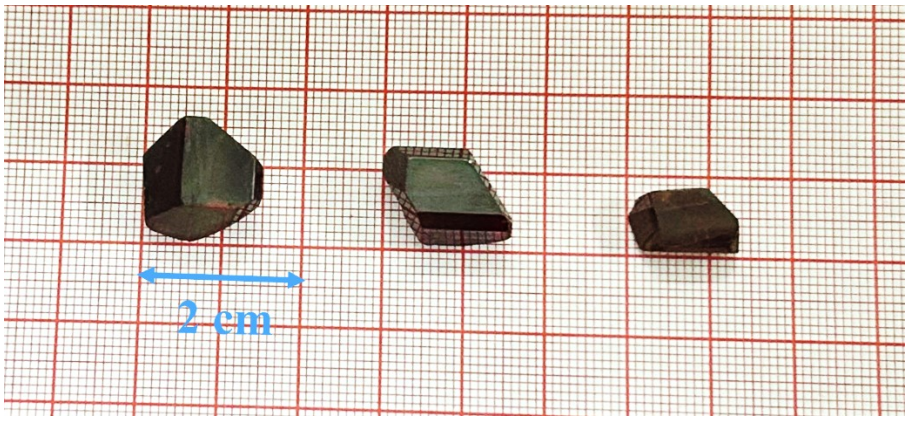

Figure S1. Block single crystals of **1** obtained by the temperature cooling method.

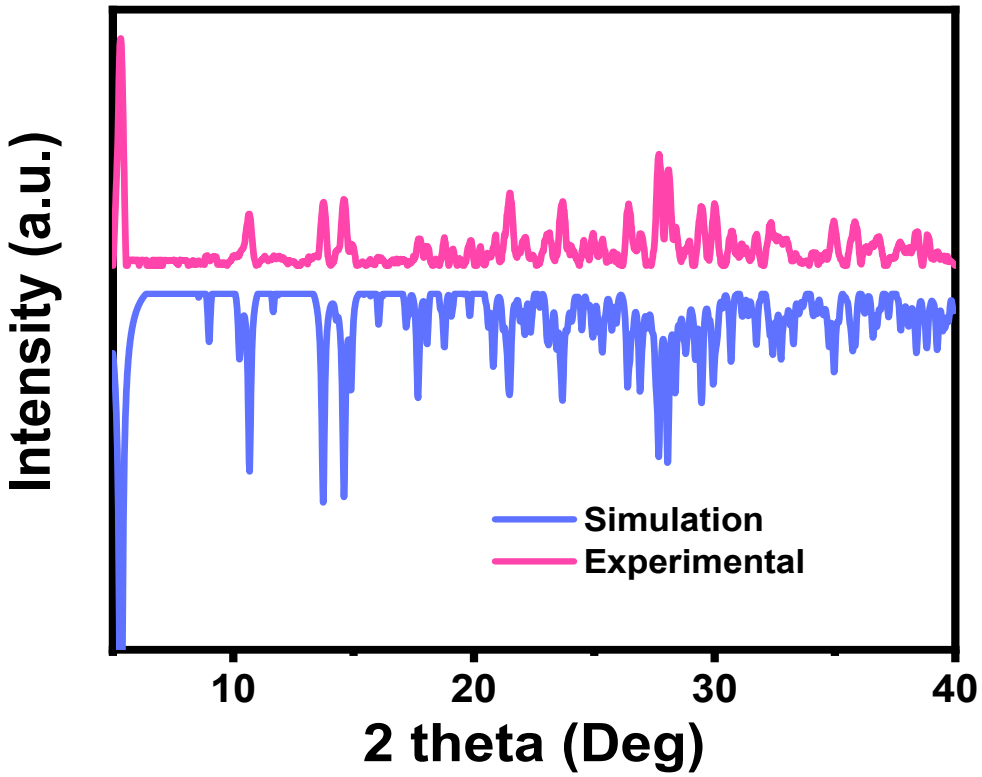

Figure S2. Experimental and simulated PXRD patterns for **1** at room temperature.

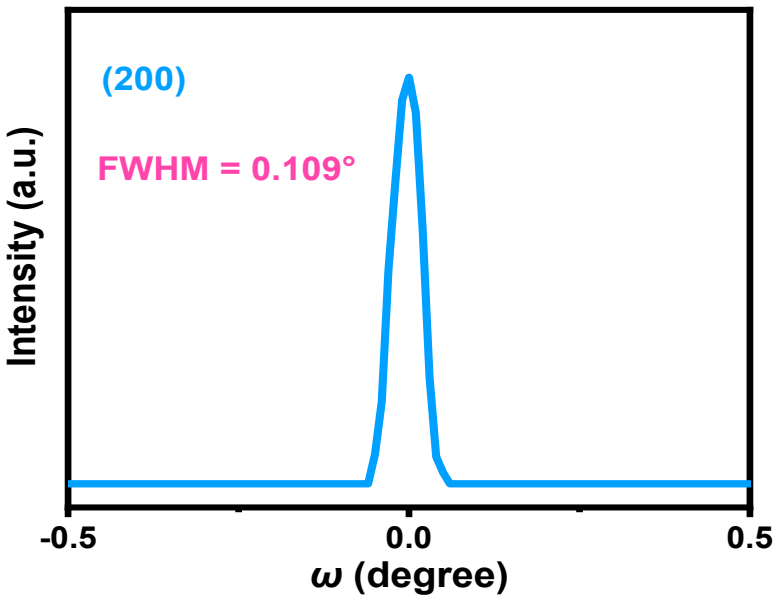

Figure S3. High-resolution XRD rocking curves for the diffraction peaks at (200).

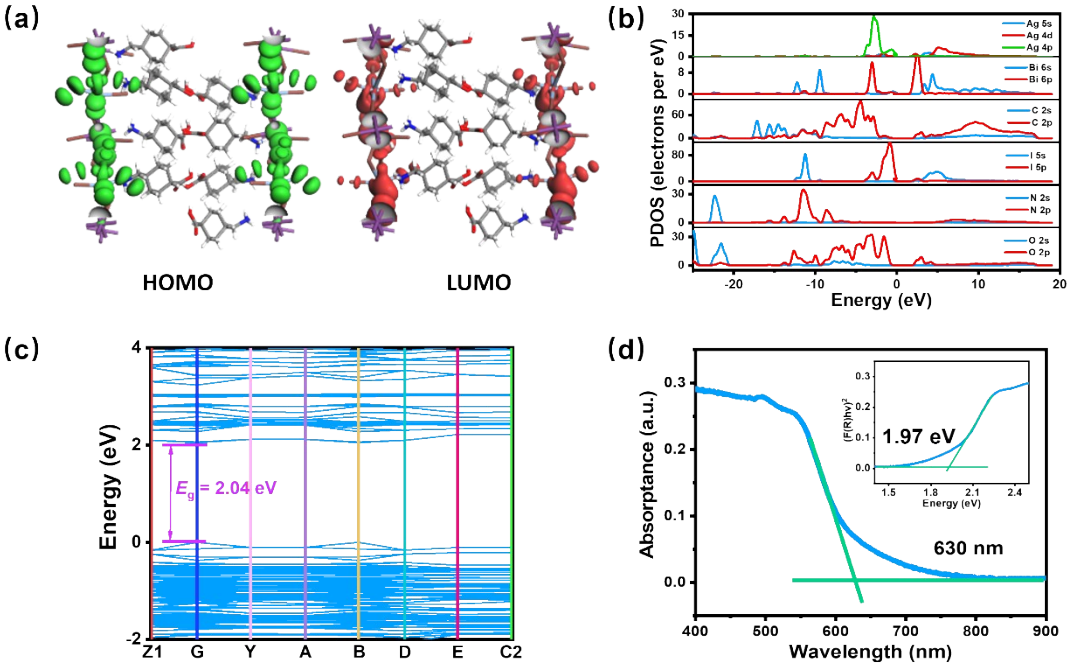

Figure S4. Optical absorption and electronic structure of **1**. The DFT calculations include (a) charge-density isosurfaces for HOMO and LUMO orbitals, (b) PDOS profiles, and (c) band structure. (d) The absorption spectrum and the estimated bandgap (inset) of **1**.

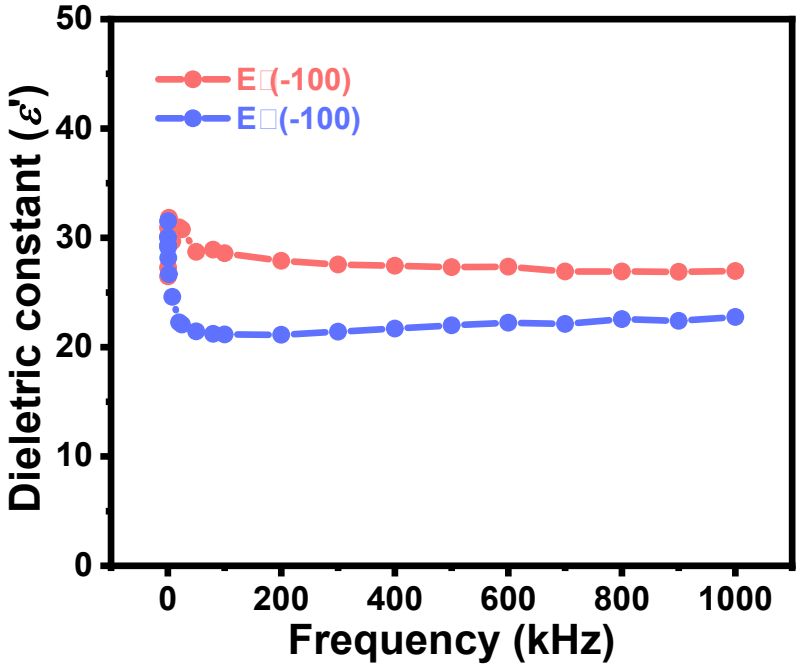

Figure S5. Frequency-dependent dielectric constant curves in both directions vertical and parallel (-100) crystal planes.

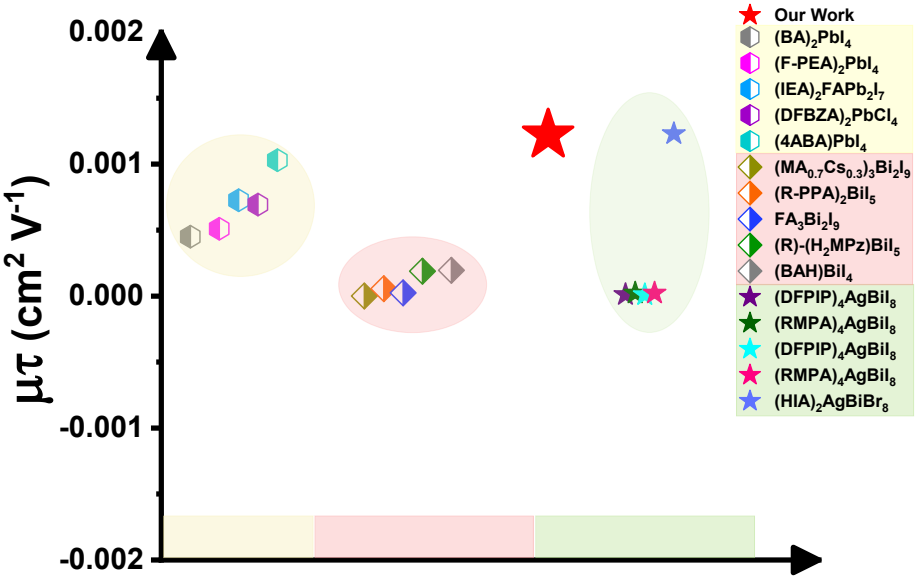

Figure S6. Photoconductivity of some reported organic-inorganic halide perovskite X-ray single crystal detectors.[1-15]

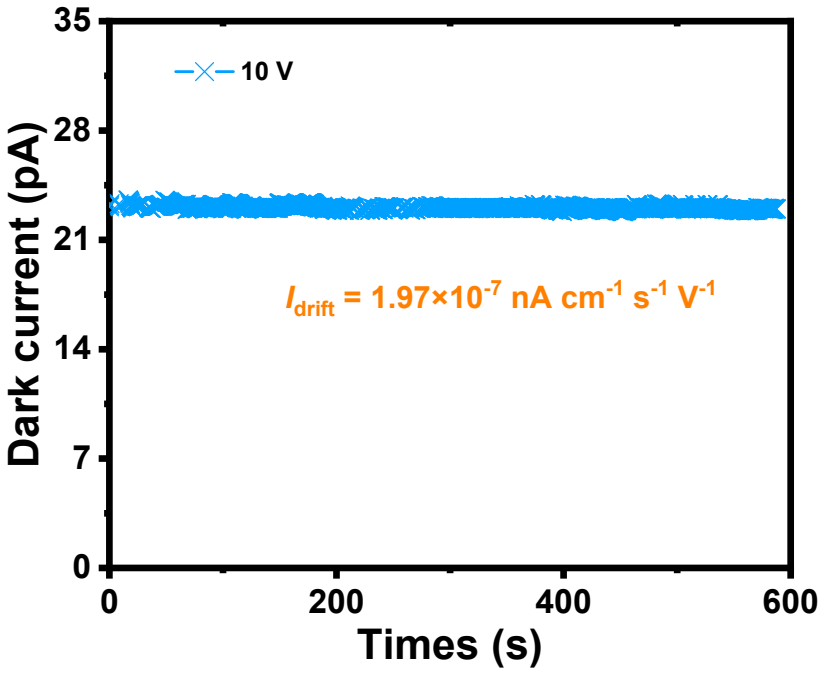

Figure S7. Dark current drift measured at 10 V bias.

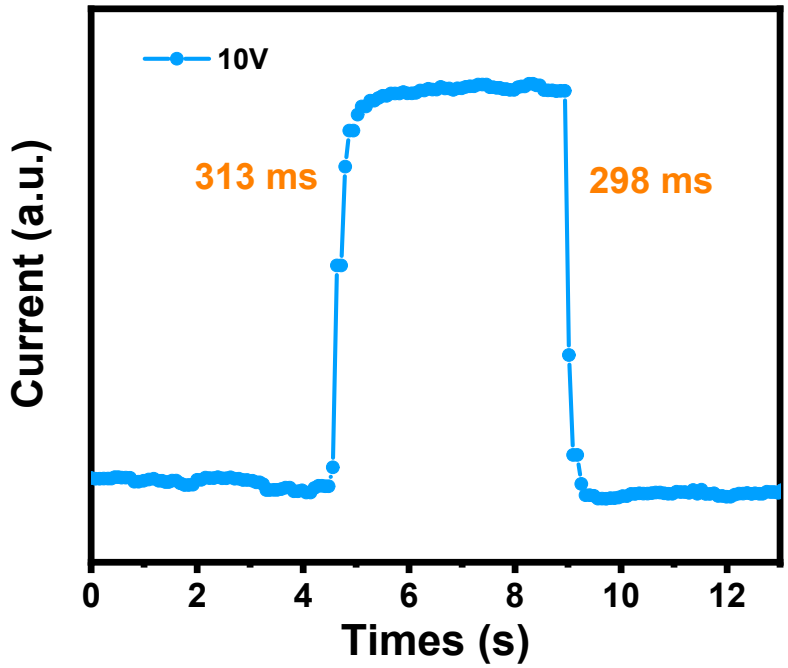

Figure S8. Response time of **1** under X-ray radiation.

Table

Table S1. Crystal data for **1** collected at 300 K

	1
Empirical formula	$C_{32}H_{66}AgBiI_8N_4O_9$
Formula weight	1982.93
Temperature (K)	300.02
Crystal system	monoclinic
Space group	$P2_1/_C$
a (Å)	16.5743(10)
b (Å)	17.0633(8)
c (Å)	19.6604(11)
V (Å^3)	5554.8(5)
Z	4
μ (mm^{-1})	8.006
F (000)	3648.0
2θ range (°)	4.786 to 50.052
Index ranges	$-19 \le h \le 19$, $-20 \le k \le 20$, $-23 \le l \le 23$
Reflections collected	88286
Independent reflections	9719[R_{int} = 0.0751, R_{sigma} = 0.0362]
Data/restraints/parameters	9719/331/506
Goodness-of-fit on F^2	1.028
Final *R* indexes [$I \ge 2\sigma$ (I)]	R_1 = 0.0457, wR_2 = 0.1052
Final R indexes [all data]	R_1 = 0.0653, wR_2 = 0.1184

Table S2. Bond lengths of crystal **1** at 300 K

Atom	Atom	Length/Å	Atom	Atom	Length/Å
Bi1	$I2^1$	3.0839(6)	C23	C20	1.522(14)
Bi1	I2	3.0840(6)	C31	C28	1.530(14)
Bi1	I3	3.0677(7)	C24	C25	1.526(15)
Bi1	$I3^1$	3.0677(7)	C2	C1	1.510(14)
Bi1	I1	3.0474(8)	C2	C7	1.532(15)
Bi1	$I1^1$	3.0475(8)	C2	C3	1.505(14)
Bi2	I4	3.0857(6)	C9	C10	1.515(13)
Bi2	$I4^2$	3.0857(6)	C32	C22	1.513(16)
Bi2	$I6^2$	3.0806(6)	C32	C18	1.488(15)
Bi2	I6	3.0806(6)	C8	C5	1.468(17)
Bi2	$I5^2$	3.0640(7)	C8	O1	1.2498(10)
Bi2	I5	3.0639(7)	C20	C21	1.510(16)
I4	$Ag1^3$	4.112(2)	C20	C19	1.508(15)
I2	$Ag1^4$	3.363(2)	C28	C29	1.501(12)
I6	Ag1	3.230(2)	C28	C27	1.501(13)
I7	Ag1	2.6772(15)	C22	C21	1.530(15)
I8	Ag1	2.6429(14)	C15	C14	1.530(16)
I3	$Ag1^5$	3.638(2)	C15	C10	1.492(15)
N3	C17	1.499(14)	C11	C12	1.539(16)
O3	C16	1.242(13)	C11	C10	1.457(15)
O5	C23	1.254(13)	C14	C13	1.531(18)
O7	C31	1.259(13)	C13	C12	1.588(18)
O4	C16	1.230(15)	C29	C30	1.526(13)
O6	C23	1.226(13)	C30	C25	1.476(14)
N2	C9	1.445(15)	C27	C26	1.511(13)
N4	C24	1.429(15)	C26	C25	1.478(14)
O8	C31	1.190(13)	C6	C5	1.526(15)
N1	C1	1.433(14)	C6	C7	1.535(14)

O2	C8	1.155(16)	C5	C4	1.568(16)
C17	C32	1.534(14)	C3	C4	1.502(14)
C16	C13	1.511(16)	C18	C19	1.532(14)

Symmetry transformations used to generate equivalent atoms: [1]2-X, 1-Y 1-Z; [2]-X, -Y, 1-Z; [3]X, 1/2-Y, -1/2+Z; [4]1-X, 1/2+Y, 3/2-Z; [5]1+X, Y, Z

Table S3. Bond angles of crystal **1** at 300 K.

Bond	Angle/°	Bond	Angle/°
I2[1]-Bi1-I2	180.00(3)	N4-C24-C25	113.2(11)
I3[1]-Bi1-I2	90.648(19)	C1-C2-C7	113.5(9)
I3-Bi1-I2	89.351(19)	C3-C2-C1	112.1(9)
I3[1]-Bi1-I2[1]	89.351(19)	C3-C2-C7	110.6(9)
I3-Bi1-I2[1]	90.650(19)	N1-C1-C2	114.1(9)
I3-Bi1-I3[1]	180.0	N2-C9-C10	113.1(10)
I1-Bi1-I2[1]	89.43(2)	C22-C32-C17	106.8(9)
I1-Bi1-I2	90.57(2)	C18-C32-C17	113.4(10)
I1[1]-Bi1-I2	89.43(2)	C18-C32-C22	109.5(10)
I1[1]-Bi1-I2[1]	90.57(2)	O2-C8-C5	126.6(12)
I1-Bi1-I3[1]	89.85(3)	O2-C8-O1	114.7(14)
I1-Bi1-I3	90.15(2)	O1-C8-C5	118.4(13)
I1[1]-Bi1-I3[1]	90.15(2)	C21-C20-C23	107.9(9)
I1[1]-Bi1-I3	89.85(3)	C19-C20-C23	114.5(9)
I1-Bi1-I1[1]	180.0	C19-C20-C21	110.0(10)
I4-Bi2-I4[2]	180.0	C29-C28-C31	114.2(10)
I6[2]-Bi2-I4[2]	89.380(18)	C27-C28-C31	109.3(9)
I6[2]-Bi2-I4	90.619(18)	C27-C28-C29	108.7(10)
I6-Bi2-I4	89.379(18)	C32-C22-C21	109.9(10)
I6-Bi2-I4[2]	90.622(18)	C10-C15-C14	110.3(10)
I6-Bi2-I6[2]	180.0	C10-C11-C12	111.0(10)
I5[2]-Bi2-I4	89.871(19)	C15-C14-C13	110.6(11)
I5-Bi2-I4	90.129(19)	C20-C21-C22	111.2(10)

I5-Bi2-I4[2]	89.870(19)	C16-C13-C14	109.1(11)
I5[2]-Bi2-I4[2]	90.130(19)	C16-C13-C12	107.4(11)
I5-Bi2-I6	89.88(2)	C14-C13-C12	107.8(10)
I5-Bi2-I6[2]	90.12(2)	C28-C29-C30	111.5(10)
I5[2]-Bi2-I6	90.12(2)	C25-C30-C29	112.0(11)
I5[2]-Bi2-I6[2]	89.88(2)	C28-C27-C26	111.3(12)
I5-Bi2-I5[2]	180.0	C11-C12-C13	109.2(11)
Bi2-I4-Ag1[3]	143.58(3)	C25-C26-C27	111.5(12)
Bi1-I2-Ag1[4]	169.13(4)	C5-C6-C7	112.6(9)
Bi2-I6-Ag1	156.91(4)	C8-C5-C6	111.0(10)
Bi1-I3-Ag1[5]	162.17(4)	C8-C5-C4	109.6(10)
I7-Ag1-I6	98.36(5)	C6-C5-C4	110.2(9)
I8-Ag1-I6	102.89(6)	C2-C7-C6	111.2(9)
I8-Ag1-I7	156.58(8)	C4-C3-C2	112.5(9)
N3-C17-C32	112.6(10)	C30-C25-C24	111.5(11)
O3-C16-C13	117.6(11)	C30-C25-C26	109.5(12)
O4-C16-O3	120.2(11)	C26-C25-C24	110.3(11)
O4-C16-C13	122.1(11)	C15-C10-C9	109.9(9)
O5-C23-C20	117.4(10)	C11-C10-C9	113.6(10)
O6-C23-O5	121.3(10)	C11-C10-C15	113.0(11)
O6-C23-C20	121.2(10)	C3-C4-C5	111.5(10)
O7-C31-C28	114.0(10)	C32-C18-C19	111.2(10)
O8-C31-O7	122.9(11)	C20-C19-C18	110.0(10)
O8-C31-C28	123.0(10)		

Symmetry transformations used to generate equivalent atoms: [1]2-X, 1-Y, 1-Z; [2]-X, -Y, 1-Z; [3]X, 1/2-Y, -1/2+Z; [4]1-X, 1/2+Y, 3/2-Z; [5]1+X, Y, Z

Table S4. Performances of some reported halide perovskite X-ray single crystal detectors.

Materials	Sensitivity ($\mu C\ Gy_{air}^{-1}cm^{-2}$)	Detection limit ($nGy_{air}S^{-1}$)	References
$MA_3Bi_2I_9$	1947	83	[16]
$Cs_3Bi_2I_9$	1652.3	130	[17]
$(MA_{0.7}Cs_{0.3})_3Bi_2I_9$	130	12.8	[6]
$(R\text{-}PPA)_2BiI_5$	150	2570	[7]
$Rb_3Bi_2I_9$	42.5	8.32	[18]
$(BAH)BiI_4$	1181.8	77	[10]
$(DFPIP)_4AgBiI_8$	188	3130	[11]
$(RMPA)_4AgBiI_8$	949.6	85	[12]
$(HIS)_2AgSbBr_8$	223	84.2	[19]
$FA_3Bi_2I_9$	598.1	200	[8]
$(DMEDA)BiI_5$	72.5	-	[20]
$(t\text{-}ACH)_4AgBiI_8{\cdot}H_2O$	3221.6	12	Our Work

Reference

[1] Yukta, J. Ghosh, M. Afroz, S. Alghamdi, P. Sellin and S. Satapathi, *ACS Photonics*, 2022, **9**, 3529.

[2] H. Li, J. Song, W. Pan, D. Xu, W. Zhu, H. Wei and B. Yang, *Adv. Mater*, 2020, **32**, 2003790.

[3] D. Fu, Y. Zhang, Z. Chen, L. Pan, Y. He and J. Luo, *Small*, 2024, 2403198.

[4] X. Zeng, Y. Liu, Y. Chen, Qi. Fan, T. Yang, L. Tang, W. Guo, Y. Ma, J. Luo and Z. Sun, *ACS Energy Lett.*, 2024, **9**, 381-387.

[5] Q. Fan, Y. Ma, S. You, H. Xu, W. Guo, Y. Liu, L. Tang, W. Li, J. Luo and Z. Sun, *Adv. Funct. Mater.*, 2024, **34**, 2312395.

[6] S. Tie, D. Xin, S. Dong, B. Cai, J. Zhu and X. Zheng, *ACS Sustain. Chem. & Eng.*, 2022, **10**, 10743-10751.

[7] S. You, Z. Zhu, S. Dai, J. Wu, Q. Guan, T. Ting, P. Yu, C. Chen, Q. Chen and J. Luo, *Adv. Funct. Mater*., 2023, **33**, 2303523.

[8] W. Li, D. Xin, S. Tie, J. Ren, S. Dong, L. Lei, X. Zheng, Y. Zhao and W. Zhang, *J. Phys. Chem. Lett.*, 2021, **12**, 1778-1785.

[9] X. Dong, J. Liang, Z. Xu, H. Wu, L. Wang, S. You, J. Luo and L. Li, *Chinese Chem. Lett.*, 2024, **35**, 108708.

[10] C. Ma, H. Li, M. Chen, Y. Liu, K. Zhao and S. Liu, *Adv. Funct. Mater.*, 2022, **32**, 2202160.

[11] C. Wang, H. Li, M. Li, Y. Cui, X. Song, Q. Wang, J. Jiang, M. Hua, Q. Xu, K. Zhao, H. Ye and Y. Zhang, *Adv. Funct. Mater*., 2021, **31**, 2009457.

[12] J. Wu, S. You, P. Yu, Q. Guan, Z. Zhu, Z. Li, C. Qu, H. Zhong, L. Li and J. Luo, *ACS Energy Lett.*, 2023, **8**, 2809.

[13] C. Wang, H. Li, M. Li, Y. Cui, X. Song, Q. Wang, J. Jiang, M. Hua, Q. Xu, K. Zhao, H. Ye and Y. Zhang, *Adv. Funct. Mater*., 2021, **31**, 2009457.

[14] J. Wu, S. You, P. Yu, Q. Guan, Z. Zhu, Z. Li, C. Qu, H. Zhong, L. Li and J. Luo, *ACS Energy Lett.*, 2023, **8**, 2809-2816.

[15] W. Guo, H. Xu, Q. Fan, P. Zhu, Y. Ma, Y. Liu, X. Zeng, J. Luo and Z. Sun, *Adv. Optical Mater.*, 2024, **12**, 2303291.

[16] Y. Liu, Z. Xu, Z. Yang, Y. Zhang, J. Cui, Y. He, H. Ye, K. Zhao, H. Sun, R. Liu, M. Liu, M. G. Kanatzidis and S, Liu, *Matter*, 2020, **3**, 180-196.

[17] Y. Zhang, Y. Liu, Z. Xu, H. Ye, Z. Yang, J. You, M. Liu, Y. He, M. G. Kanatzidis and S. Liu, *Nat. Commun.,* 2020, **11**, 2304.

[18] M. Xia, H. Yuan, G. Niu, X. Du, L. Yin, W. Pan, J. Luo, Z. Li, H. Zhao, H. Xue, X. Miao and J. Tang, *Adv. Funct. Mater*., 2020, **30**, 1910648.

[19] Q. Fan, H. Xu, S. You, Y. Ma, Y. Liu, W. Guo, X. Hu, B. Wang, C. Gao, W. Liu, J. Luo and Z. Sun, *Small*, 2023, **19**, 2301594.

[20] L. Yao, G. Niu, L. Yin, X. Du, Y. Lin, X. Den, J. Zhang and J. Tang, *J. Mater. Chem. C.,* 2020, **8**, 1239-1243.